Discharge Characteristics of Bubbles at the Interface between AlN Ceramic and FC-72 Liquid

Shenyang Mo, Xuebao Li, *Member, CSEE*, Zhibin Zhao, *Member*, *IEEE* and Xiang Cui, *Senior Member, IEEE*

***Abstract*—In order to evaluate the insulation of two-phase immersion cooling in the HV power electronic package, the insulation degradation of the dielectric interface induced by bubbles is investigated. In this paper, a test strategy with 50 Hz unipolar DC and AC combined voltage for partial discharge (PD) at boiling interface of AlN ceramic. The insulation threshold of an AlN ceramic surface is acquired in several dielectric environments, such as air, FC-72 liquid (FC-72, a Fluorinert^{TM} from 3M^{TM}), FC-72 vapor, and boiling state of FC-72. This reveals the deterioration of boiling on the insulation of the surface immersed in the dielectric refrigerant. To investigate the mechanism of the PD feature at the boiling interface, the PD patterns of the unrestricted bubble and the accumulated bubble are acquired and contrastively analyzed. Combined with the feature of the back discharge and the bubble behavior, the charged vapor-ceramic interface-is relatively stable due to the accumulated vapor layer. This stability of the charged vapor-ceramic interface is broken if the bubble is unrestricted. Besides, it is discovered that the vapor-liquid interface inside the bubble may be another charged interface, which can also trigger a back discharge.**

***Index Terms*—partial discharge, bubble, surface discharge, FC-72, two-phase cooling, biased AC voltage, power electronic package**

I. Introduction

TWO-PHASE immersion cooling has remarkable advantages in the heat dissipation. It is also an ideal technique for cooling HV power electronic devices [1]. However, appearance of thermal bubbles is a typical insulation challenge, which limits the application of the two-phase cooling technology in high electric field condition. The insulation ability and characteristic need more investigation for the insulation design in HV two-phase environment.

As for the electric structure in HV power electronic package, the dielectric interface, such as the passivation layer of the die [2, 3] and the ceramic surface of DBC (Direct Bond Copper) [4], should be paid more attention for insulation design. In the immersion environment with the refrigerant, the power heat of the die makes the refrigerant vaporize and induces boiling on the surface. The occurrence of the bubble enhances the electric field along the interface, which may stimulate ionization along the dielectric surface inside the bubble [5] and degrades the insulation ability of the interface. The similar degradation exists at the interface between the ceramic and the silicone gel in power electronic package [6]. Thus, the effect of the dynamic bubbles on the insulation interface needs further research.

The bubble-induced discharge characteristic has been investigated mostly in a liquid environment. It can be ignited by both anode electric stress and cathode stress [7]. Except for the research of the streamer characteristic inside the single bubble [8, 9], the PD pattern of the bubble flow in dielectric liquid has be analyzed in the previous work [10], which reveals the mechanism of the discharge behavior inside the bubble cluster.

As a major insulation structure in the package of power electronic devices, the surface discharge characteristic is explored at several dielectric interfaces. For example, the rules of back discharge have been modeled with the semi-square voltage on the PEEK (Polyetheretherketone) surface [11], which is used as the framework material for a press-pack submodule. The cavity effect on interface insulation is also a specific condition for the silicone gel in the power module. S. Nakamura et al proceed a PD research with a repetitive impulse voltage on the interface between the glass substrate and the silicone gel [12]. It also reflects the modified behavior induced by charged surface inside a cavity.

However, different from the fixed cavity in silicone gel, the thermal bubble in liquid shows the dynamic behavior. In order to evaluate the insulation effect of the thermal bubbles on the interface, it is intended to set up a test for investigation of boiling interface. Moreover, we contrast the insulation characteristic of ceramic surface in air, FC-72 vapor, FC-72 liquid, and its boiling state, respectively. The PD patterns under different bubble behaviors are contrastively analyzed. According to the discharge characteristics under several interface conditions, their PD thresholds and the particularity of discharge characteristic on boiling interface are discovered. Moreover, the mechanism of the specific characteristics of boiling interface is revealed, which is further confirmed with the response time of the back discharges.

II. Measuring Methods and Experimental Setup

The unipolar voltage likes the semi-square voltage or the DC is more consistent with the application of the power electronic package. But it is not convenient to identify the discharge mechanism, especially when the bubbles exist. The traditional PD method with 50Hz AC voltage is maturer for the PD

This work was supported by the National Natural Science Foundation of China-State Grid Corporation Joint Fund for Smart Grid (No. U1766219).

S. Y. Mo, X. B. Li (corresponding author, e-mail: lxb08357x@ncepu.edu.cn), Z. B. Zhao, and X. Cui are with State Key Laboratory of Alternate Electrical Power System with Renewable Energy Sources, North China Electric Power University, Beijing 102206, China.

DOI: 10.17775/CSEEJPES.2021.00410

identification. Thus, the 50 Hz unipolar DC- AC combined voltage is imposed in the PD test here, which is also a common strategy for PD test in power electronic package [2,13]. It is convenient to reflect the charge modulation on the surface with a unipolar test voltage. Besides, the result from the unipolar voltage is much more preferable for the further insulation research of the two-phase cooling package in power electronic devices.

Fig. 1(a) illustrates the test setup. The voltage is amplified 2000 times by the Matsusada voltage amplifier and applied to the test chamber. The 50 Hz AC signal is biased to unipolarity by the signal generator before amplification. The minimum test voltage can be maintained at 100±5 V, while the maximum can reach 20kV. The test voltage mentioned hereafter is the peak value V_p

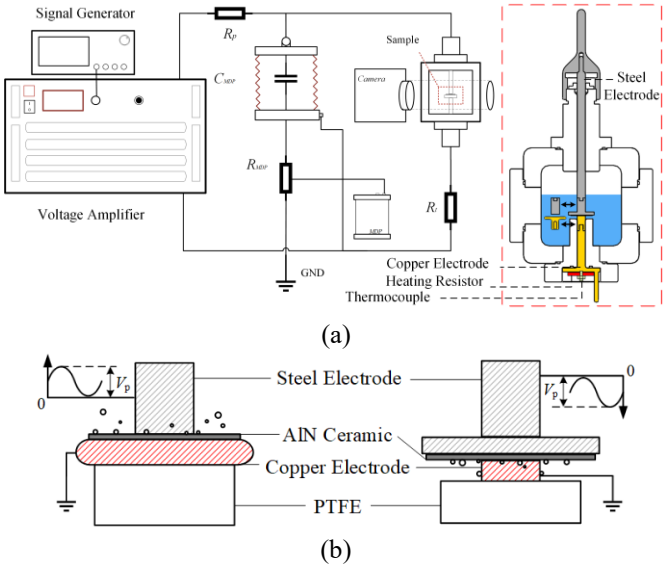

Fig. 1. PD measurement system for the bubble interface.
(a) Schematic diagram of platform, (b) Schematic diagram of samples

The Omicron MPD 600 basing on IEC 60270 standard is used for the PD measurement. The coupling device of the PD test system is connected in series with a 1 μF coupling capacitor. Besides, the behavior of the bubble at the interface can be observed and analyzed through the shadowgraph, which is captured with a Canon 1DX digital camera and a parallel light source.

Fig. 1(a) illustrates the chamber geometry. The heat is conducted to the dielectric surface through the copper electrode. The geometry of the electrode is adjustable through the replacements of the copper and steel electrode to realize two bubble-generate method. A heating resistor is attached on the external bottom of the copper electrode to heat the AlN sample. The temperature of the copper electrode is maintained at 140°C by a thermocouple to makes the boiling stable.

The AlN ceramic, which is used as an advanced insulation and heat-conductive material in the DBC, is chosen as the sample layer. This can simulate the dielectric environment in the package of the power electronic module as closely as possible. In the package, the dies are sintered on the DBC, which is the main structure for cooling. Since the other side of the dies is covered with the silicone gel, this structure can only provide a single-sided cooling for the dies. This limitation can be improved by replacing the silicone gel with the refrigerant for the two-phase cooling. However, the refrigerant will be heated to boil, which cools the dies with the latent heat of vaporization. The thermal bubbles induced by boiling can immediately detach from the interface, or accumulates on the interface if the DBC is placed in reverse.

Referring to the situations that the bubbles may appear on the interface in the application, two generation methods of the bubbles are realized as shown in Fig. 1(b), which is defined as the unrestricted bubble and the accumulated bubble, respectively.

The dynamic behavior of the unrestricted bubble and the accumulated bubble are shown in Fig. 2. As for the unrestricted bubble, the center of ceramic is covered with the steel rod electrode, where the cooling efficiency is lowest since the thermal conductivity of stainless steel is low. The temperature of ceramic surface around the rod electrode is relatively higher than other area on the ceramic surface. Therefore, it can be observed from Fig. 2 (a) that the bubbles are generated continuously here and rise along the rod electrode. Then, the bubble may also generated from the other exposed ceramic surface, as well as copper surface of plane electrode, which immediately detach from the ceramic surface as shown in Fig. 2(a).

While, for the accumulated condition, the bubbles generate from the surface of the copper electrode and accumulate on the lower surface of the ceramic. Due to the thermal conductance of the AlN ceramic, few bubbles can also grow directly from the ceramic surface. Based on the differences in the size and mobility under the two bubbles states, it is feasible to identify the mechanism through the distinctions in the PD characteristics.

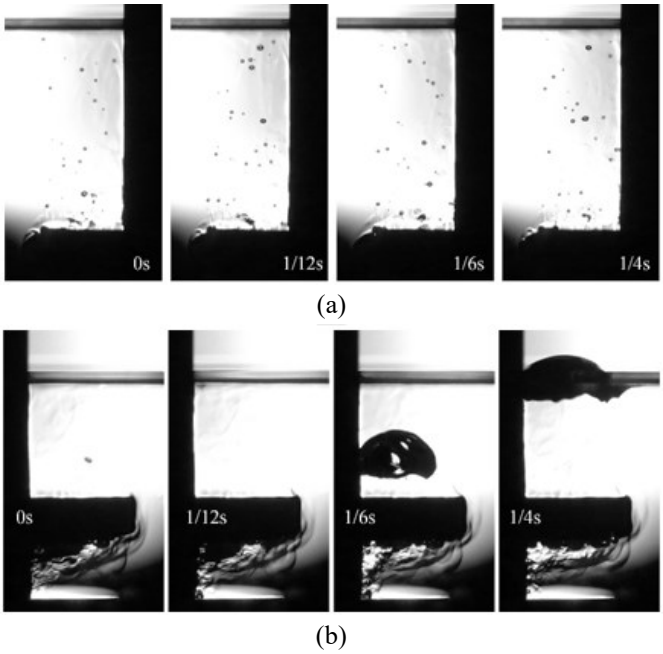

Fig. 2. Bubble dynamic in time sequence under 0V under unrestricted condition (a) and accumulated condition (b).

In order to unify the streamer polarity, for the unrestricted condition, the rod electrode is applied with the positive DC-AC

combined voltage, and the plane electrode is grounded. As for the accumulated condition, the plane electrode is applied with the negative DC-AC combined voltage and the plane electrode is grounded.

III. Experiment Results and Analysis

In this chapter, the PD patterns of the air-ceramic interface are indicated first to show the modulation mechanism on the charged interface under the 50 Hz unipolar DC- AC combined voltage. Compared with the result in the liquid environment, it can be speculated that the discharge occurs in the bubble when boiling. Then, we contrastively analyze the PD patterns in two bubble states.

According to the contrast between the partial discharge inception voltages (PDIV) in air, FC-72 liquid, and its boiling phase, the insulation characteristic in the refrigerant and the two-phase cooling condition can be evaluated. Finally, a brief statement is given about the surface-discharge experiment in FC-72 vapor to provide a criterion of discharge inception for further analysis.

A. PD characteristic of the air-ceramic interface

In order to cognize the mechanism of surface discharge under unipolar voltage, a PD experiment at the air-ceramic interface is helpful for the analysis of the discharge characteristic of a boiling interface. Without the FC-72 refrigerant, the PD feature of the ceramic surface is firstly tested in air environment. The PDIV of the air-ceramic interface is tested as 2.4 kV. All the PDIV results in this research are determined by the cumulative probability of 63%. The phase-resolved partial discharge (PRPD) under 2.6 kV and 3.1 kV are given in Fig. 3. According to the observation of the PD pattern during the voltage raising, the development of PD can be divided into two stages.

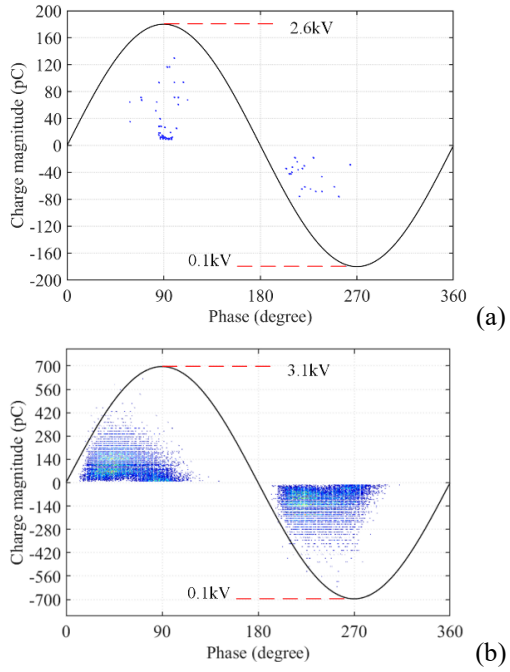

Fig. 3. PRPD pattern of the ceramic surface in air under (a) 2.6 kV and (b) 3.1 kV.

As demonstrated in Fig. 3(a), the discharge pulse occurs initially at 90° once the voltage exceeds PDIV, accompanied by a few negative discharges between 180-270°. Then, the PD frequency increases sharply and tends to stable as the voltage raises. The phase interval of positive discharge gradually shifts forward to 0-90°. The PD pattern of positive discharge tends to be similar to that of negative discharge in the PRPD pattern-as shown in Fig. 3(b).

In Fig. 3(a), it can be confirmed that the discharges occurring around 90° is triggered by the high electric field when the voltage exceeds PDIV. However, the field strength is not enough anymore to trigger the ionization around 270°. The polarity of discharges between 180-270° is also different from the electric field. This phenomenon reflects the existence of surface charge. The discharge occurring between 180-270° is back discharge. It is triggered by the inversed field, which is contributed by the charge trapped on the surface [11].

At the beginning of the PD inception, the surface charge is little to affect the next forward discharge. However, this effect will be gradually obvious as the voltage increases or the discharge accumulates. As reflected in Fig. 3(b), the phase of the forward discharges moves forward and distributes nearly between 0-90°. This reveals the field modulation of surface charge in successive voltage period, which would be a key inspiration for the analysis of the PD pattern inside the bubble hereafter.

Besides, it should be indicated that there is no PD occurs in pure FC-72 liquid until the ceramic sample is directly breakdown at 15.2 kV. Thus, the upper limit of the test voltage is 14 kV in the following experiment.

B. PD pattern of the interface with accumulated bubble

Fig. 4 shows the accumulation of the bubble. In this paper, the exposure time of the single picture is all 1/3000 s. The bubbles are generated from the copper electrode and a little ceramic surface around the copper electrode. Then, the bubbles accumulate on the lower surface of the ceramic sample. Most of the bubbles gather at the root of the copper electrode when no voltage applying. While the accumulation behavior will be affected by the electric field as shown in Fig. 4(b). The bubbles are driven to the edge of the ceramic under 14 kV, which makes the bubble distribution more uniform and consecutive on the surface.

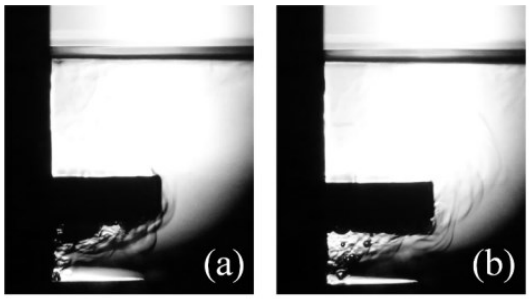

Fig. 4. Flow patterns of accumulated bubbles under (a) 0 kV and (b) 14 kV.

The surface within the bubbles can be regarded as an interface between the ceramic and the FC-72 vapor. Since few bubbles leave the surface until a certain accumulation, this

interface is relatively uniform and stable.

The PD characteristic in this condition is illustrated in the PRPD pattern as Fig. 5(a), which can be post processed to a phase-resolved of PD number (PRPDN) as Fig. 5(b). Another two PRPDN patterns under 10 kV and 12 kV are also superimposed in Fig. 5(b) to shows the development of patterns as voltage raises.

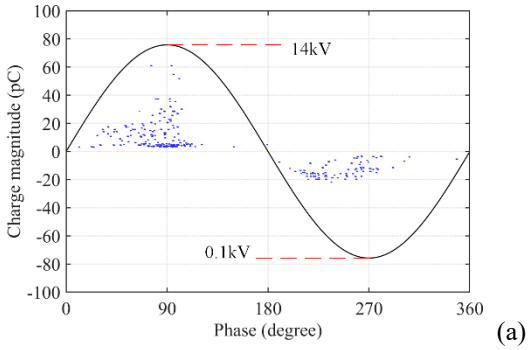

(a)

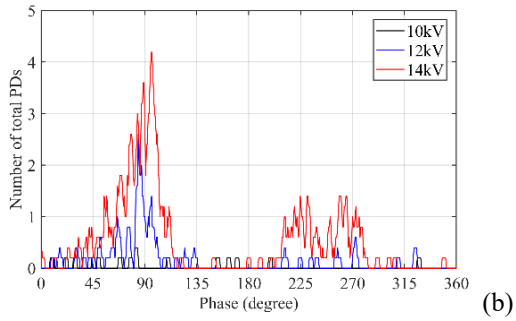

(b)

Fig. 5. PD patterns of the interface with accumulated bubbles.
(a) PRPD pattern under 14 kV, (b) PRPDN patterns under 10 kV, 12 kV, and 14 kV.

Since there is no discharge in liquid environment before 14 kV, it can be speculated that the discharge only occurs in bubble, which can be regarded as a vapor void in the liquid. The PRPD pattern in Fig. 5(a) is similar to the discharge characteristic at the air-ceramic interface. On the one hand, most of PDs distribute between 0-90° and 180-270°. It implies a relatively stable interface, which leads to a steady effect of surface charge in successive voltage period.

On the other hand, the pattern likes Fig. 3(a) is also imposed in Fig. 5(a), which shows the PDs occurring around 90°. This also reflects the turbulence behavior of the accumulated bubble at the interface, which makes the effect of surface charge produced by back discharge random. For example, when the forward discharge occurs in a new-created bubble, it cannot be modulated by the surface charge in another existing bubble.

As illustrated in Fig. 5(b), the PD is more frequent as the voltage raises. While the PD patterns and their phase distributions show a similar characteristic under different voltages, which indicates the repeatability of test results under such a dynamic bubble behavior.

C. PD pattern of the interface with unrestricted bubble

Fig. 6 shows the bubble motion under unrestricted conditions. The exposure time of the single picture is also 1/3000 s. To make the bubble trajectory more apparent under such a dynamic behavior, Fig. 6 is superimposed shadowgraphs stacked by 60 continuous photos captured in 12 fps. Almost all the bubbles grow and immediately detach from the ceramic surface. Thus, the time bubble attaching on the surface is much less than the accumulated bubble. The area of the vapor-ceramic interface, which attributes to the bubble size and distribution, is also smaller and scattered.

In Fig. 6(a), it can be observed from the bubble trajectory that, the bubbles uniformly distribute upon the surface when no voltage applying. While the effect of electric stress on the bubble is similar to accumulated condition. In Fig. 6(b), the bubbles generating from the surface adjacent to the electrode are driven away from the root of the electrode. The trajectory of the bubbles appears more random compared with Fig. 6(a). This impact will be modeled and analyzed in the next chapter.

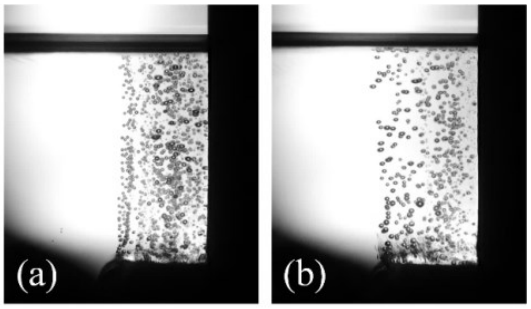

Fig. 6. Flow patterns of unrestricted bubbles under (a) 0 kV and (b) 14 kV.

The PD patterns of the interface with unrestricted bubbles are indicated as Fig. 7. The charge magnitude of PD in the unrestricted bubble is generally smaller than that in the accumulated bubble in Fig. 5(a). This is consistent with the rules in PD characteristic of bubble flow [10]. The streamer propagation would be limited by the bubble size [14]. Therefore, the charge magnitude inside the accumulated bubble is larger due to the wider ceramic-vapor interface.

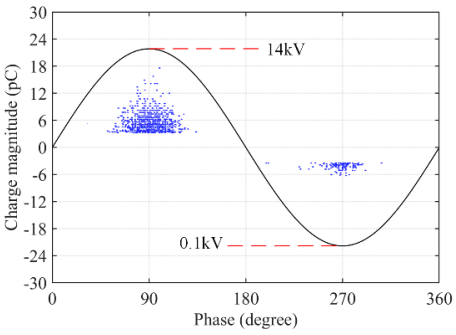

(a)

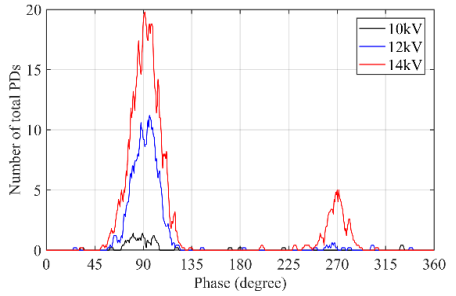

(b)

Fig. 7. PD patterns of the interface with unrestricted bubbles.
(a) PRPD pattern under 14 kV, (b) PRPDN pattern under 10 kV, 12 kV, and 14 kV.

The occurrence of back discharge still reveals a charged interface. The background electric field along this interface may decrease. Then, the inversed field ~~is~~ induced by the surface charge dominants and triggers another reversed ionization.

However, different from the PD pattern of the accumulated bubble, the forward discharges and back discharges distribute around 90° and 270°, respectively. In Fig 6(b), the forward discharge is still determined by the overstressing of the background electric field. The phase of forward discharge reflects little modulation effect of surface discharge, which means there is no charge trapped on the path of a novel streamer triggered by the background field.

It is a paradox for the classical theory of surface discharge. The PD patterns of two bubble states reflect the existence of a charged interface. While the interface charge did not affect the forward discharge in the unrestricted bubble. Thus, it still needs to analyze the behavior of the charged interface combined with the bubble motion.

In addition, it is observed that the bubbles just leaving the ionization area may distort, or even cracks after PDIV. The surface tension and pressure are two factors that maintain the shape of the bubble. However, the electric field can distort the bubble based on the difference between the permittivity of the dielectric [15]. When ionization occurs in the bubble, the plasma will make the bubble as a conductor, whose permittivity can be regarded as infinite. The severe distortion will break the surface balance and makes the bubble crack into several parts. Thus, the bubbles shown in Fig. 8 confirm the ionization inside the bubble.

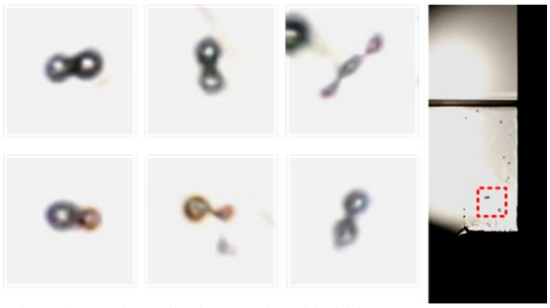

Fig. 8. Distortion and crack of unrestricted bubble.

It should be indicated that, although the PD pattern of interface with two bubble states is different, the PDIVs of them are similar due to the uniform streamer polarity and the same dielectric interface. The discharges under two conditions both incept about 10 kV.

D. PD threshold of the interface between the AlN ceramic and the FC-72 vapor.

Before further discussion, it is necessary to acquire the threshold of ionization inside the bubble. The ceramic surface inside the bubble is simplified to an interface between the AlN ceramic and the FC-72 vapor. Then, the PDIV of the ceramic surface in the vapor environment is used to get the inception electric field through the FEM (Finite Element Method).

The test chamber can form an environment with FC-72 vapor by heating the liquid. In order to ensure a pure vapor environment, it should be vacuumed first before injecting the liquid. The PDIVs of the interface between the ceramic and the FC-72 vapor is listed in Table 1.

TABLE I
PDIVS OF THE INTERFACE BETWEEN THE ALN CERAMIC AND THE FC-72 VAPOR.

Number	PDIV/kV (Peak value at 1 atm)
1	12.2
2	11.77
3	11.83
4	10.97
5	10.49

The PDIV at 1atm is determined as 11.5 kV. Besides, Fig. 9 illustrates the PRPD pattern of the vapor- ceramic interface. It also reflects the back discharge and the modulation effect of surface charge, which is similar with the air-ceramic interface.

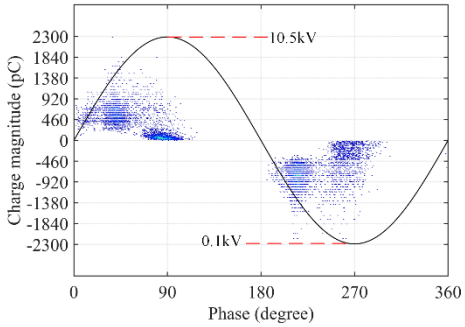

Fig. 9. PRPD pattern of the ceramic surface in FC-72 vapor under 10.5 kV.

However, since the PDIV in vapor is much higher than that in air (2.4 kV), there is almost no first stage like Fig. 3(a). The phase of PD reflects a strong modulation effect of surface charge immediately after PDIV. The charge magnitude and the PD frequency are also extremely high once the PD incepts.

IV. DISCUSSION

A. Inception criteria of PD on the boiling interface

According to the PDIV acquired at the vapor-ceramic interface mentioned above, the threshold of ionization can be determined with a critical field strength E_c by FEM, which is calculated to be 39 kV/mm. The geometry of calculation for electric field distribution is schematically illustrated in Fig. 10. The parameters of the electrode and the ceramic sample is set following the size of the test structure. The insulation interface in Fig. 10, which means the upper interface between the ceramic and FC-72, is partly meshed in μm level for precision calculation of electric field. The relative permittivity of AlN and FC-72 liquid are 9 and 1.75, respectively

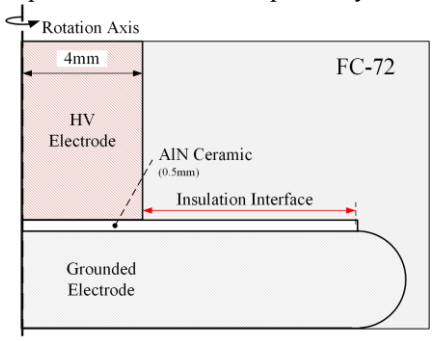

Fig. 10. Geometry for electric field analysis.

The distribution of tangential electric field along the insulation interface is indicated in Fig. 11(a). The Ionization area on the interface is determined by comparing the background electric field and the critical field strength E_c of the vapor-ceramic interface.

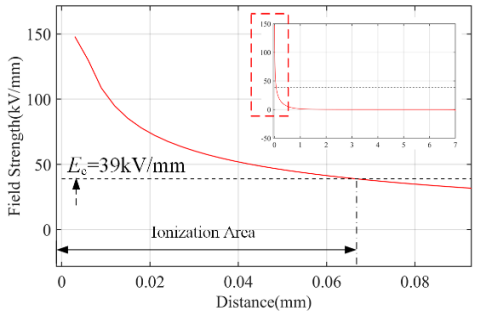

(a)

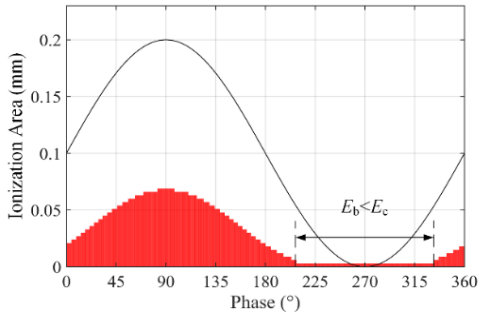

(b)

Fig. 11. Electric field distribution on the interface.
(a) Field distribution along the radius of insulation interface under 14 kV, (b) Phase distribution of ionization area during a voltage cycle (V_p=14 kV).

Then, the length evolution of the ionization area during a voltage period is acquired in Fig. 11(b). It indicates that the longest distance of the ionization range is only about 0.07 mm. While the diameter of the bubbles is measured to be 0.1-0.7mm, which means that the forward discharge can only be triggered inside the bubble produced or accumulated at the root of the electrode. In addition, the ionization area between 210-330° is zero. It reflects an interval where the background electric field is insufficient to trigger the ionization. Thus, the PD occurring in this interval is the back discharge induced by the inversed field of the charged interface.

It should be noted that the electric field inside the bubble should be enhanced since the difference between the polarization of the dielectrics. As for the spherical bubble, there is already a model for converting the electric field from the liquid into the bubble [9]. However, the geometry of the bubble attaching to the interface is irregular. It is a composite dielectric environment with two dielectrics when considering the boundary condition of the bubble.

In the bubble attaching to the ceramic surface, the tangential electric field is not affected by the ceramic, which can be expressed as

$$\frac{\partial \varphi_{vapour}}{\partial t} = \frac{\partial \varphi_{ceramic}}{\partial t} \tag{1}$$

where t indicates the tangential component of the ceramic interface. Thus, the tangential electric field along the ceramic surface inside the bubble is only determined by the permittivity of FC-72 liquid and vapor (regarded as 1). Due to the small difference between the permittivity of liquid and vapor, the deviation of the tangential field strength inside the bubble is estimated to be less than about 16% [9]. It can be ignored here in the absence of a suitable analytical model for the field transformation.

B. Mechanism of back discharge inside the accumulated bubble at the interface

As mentioned above, the PRPD pattern of the interface with the accumulated bubble reflects a PD feature similar to a standard gas-solid interface. Besides, according to the observation of bubble behavior, the accumulated bubble can nearly cover the ceramic surface, which forms a quasi-stable interface between the ceramic and the vapor. Thus, the PD mechanism inside the accumulated bubble can be partially regarded as a quasi-steady interface, which is schematically indicated in Fig. 12.

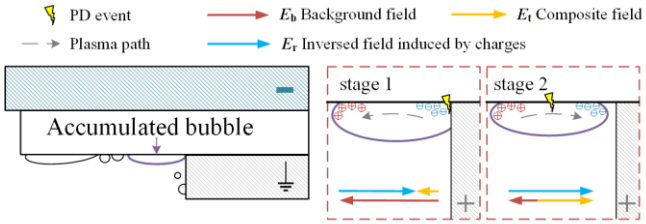

Fig. 12. Schematic diagram of back discharge in accumulated bubbles at the interface.

First, in stage 1, the background field E_b dominated by the applied voltage reaches and exceeds the critical field strength of the vapor-ceramic interface. A forward discharge is triggered by the background field. the positive and negative ions induced by plasma are trapped on the surface, which builds an inversed field E_r on the surface equivalent to the background field strength E_b. Then, in stage 2, the voltage decreases after the peak, the inversed field E_r tends to dominate and induce a back discharge. The composite field strength E_t, which is composed of the E_b and E_r, should satisfy the condition for detrapping of the surface charge, or exceed the critical field strength E_c to triggered another ionization.

Since the residence time of the bubble is much longer than a voltage period, the novel distribution of ions induced by back discharge will modulate the composite field E_t in the next voltage cycle. It makes the phase of forward discharges in PRPD deviate forward as Fig. 5.

However, if the bubble detaches from the root of the electrode in successive periods, as indicated in stage 2 of Fig. 12, the field condition for a new ionization may not be satisfied anymore. The next forward discharge may occur in another bubble, where no charge is trapped and no inversed field built. This may cause the unmodulated forward discharge in PRPD as Fig. 5(a).

The stability of the charged interface can be revealed by response time of the back discharge t_r, which is defined as the time interval between a back discharge and its previous adjacent forward discharge. Based on the record of PD sequence and their polarity, the t_r can be summarized into a

probability distribution. According to a statistics of all the back discharges in Fig. 5(a), the probability of the t_r at the interface with the accumulated bubbles is summarized in Fig. 13.

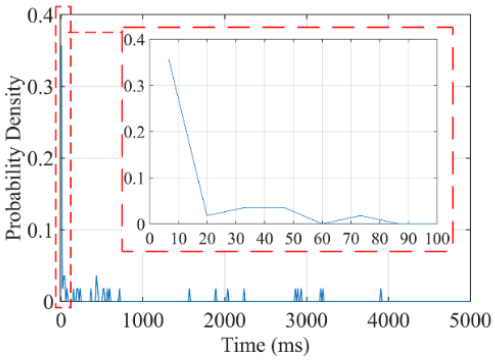

Fig. 13. Probability distribution of t_r within the accumulated bubbles.

Nearly 30% of the back discharge, whose t_r is shorter than 20 ms, occurring during one voltage cycle after the adjacent forward discharge. This feature is almost consistent with the PD mechanism of the conventional gas-solid interface. It reflects a quasi-steady interface during the successive periods in an accumulated bubble.

C. Mechanism of back discharge inside the unrestricted bubble at the interface

It is discovered that the charged interface does not modulate the electric field, which reflects no phase deviation as Fig.4. Based on this difference between the PD patterns of the accumulated bubbles and the unrestricted bubble, it is necessary to reveal the particular mechanism in the PRPD pattern of the interface with the unrestricted bubble.

According to comparing the behavior between two bubble states, the unrestricted bubble is more detachable, which makes the vapor-ceramic interface unsteady. This behavior is more obvious in the electric field. Thus, the dynamic behavior of the charged interface needs to be analyzed hereafter combining with the bubble motion based on an analytical model as

$$m_{eff}\frac{\mathrm{d}\boldsymbol{v}}{\mathrm{d}t}=\boldsymbol{F}_{\mathrm{b}}+\boldsymbol{F}_{\mathrm{d}}+\boldsymbol{F}_{\mathrm{e}} \tag{2}$$

$$m_{eff}=\frac{4}{3}\pi r^3(\rho_g+\frac{1}{2}\rho_l) \tag{3}$$

where m_{eff} is the effective mass of the bubble, r is the radius of the bubble, ρ_g and ρ_l is the density of the FC-72 vapor and liquid, respectively. Regardless of the turbulence effect on the bubble, three forces, the buoyancy force $\boldsymbol{F}_{\mathrm{b}}$, drag force $\boldsymbol{F}_{\mathrm{d}}$ and dielectrophoretic force $\boldsymbol{F}_{\mathrm{e}}$ determine the trajectory of the bubble [16], which can be expressed as

$$\boldsymbol{F}_{\mathrm{b}}=[\frac{4}{3}(\rho_g-\rho_l)\pi r^3]\boldsymbol{g} \tag{4}$$

$$\boldsymbol{F}_{\mathrm{d}}=-4\pi\mu r\boldsymbol{v} \tag{5}$$

$$\boldsymbol{F}_{\mathrm{e}}=2\pi r^3\frac{\varepsilon_l(\varepsilon_g-\varepsilon_l)}{2\varepsilon_l+\varepsilon_g}\nabla E^2 \tag{6}$$

where ε_l and ε_g are permittivity of the liquid and vapor FC-72, respectively. μ is the dynamic viscosity of FC-72 liquid.

The effect of electric field on the bubble can be summarized in electrophoretic force and dielectrophoretic force. The former is Colom force, which only acts on charged bubble. The latter force is mainly due to the polarization of bubble in non-uniform field [17]. These forces and the bubble dynamic motion are schematically illustrated in Fig. 14.

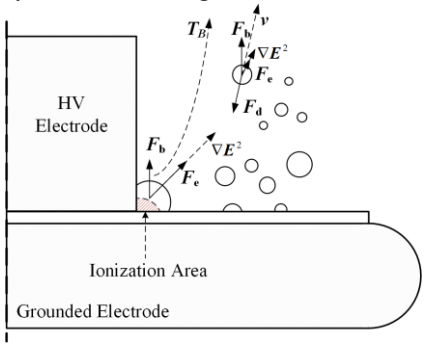

Fig. 14. Schematic diagram of dynamic motion of the bubble.

In the following analysis, it is believed that the discharge occurs along with the interface inside the bubble before detachment. Moreover, it is estimated that the vapor-liquid interface inside the bubble may also be charged after a forward discharge. Thus, the Coulomb force acting on the floating charged bubble should be another factor that affects the bubble behavior.

However, the Coulomb force only affect a few charged bubbles. The charge magnitude inside the bubble is also hard to evaluate. Therefore, the Coulomb force, which is ignored in the model, is only quantitatively considered in the following analysis. Taking the bubble whose radius is 0.1 mm as an example, the trajectory simulation of bubble flow is illustrated in Fig. 15.

The simulated trajectory is similar to the feature of the bubble flow in Fig. 6(b). It reflects the impact of the electric field on the bubble under the non-uniform electric field. The bubbles generating around the electrode are driven away from the ionization area by the dielectrophoretic force within 5 ms. Besides, since the direction of the electric field is similar to the dielectrophoretic force, the Coulomb force will strengthen this impact for the charged bubble. It means the background field inside the bubble may drop rapidly within 1/4 voltage cycle, which satisfies the field criteria for the back discharge along with the interface.

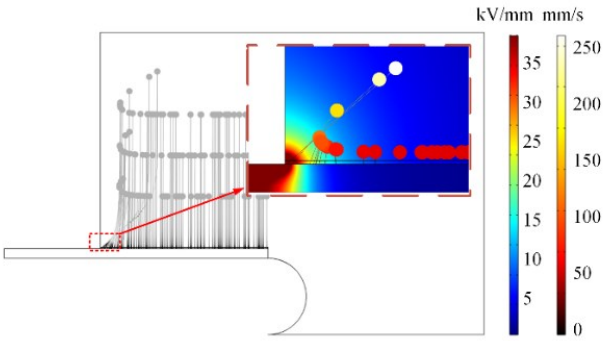

Fig. 15. Calculation result of the bubble trajectory and the transient moment at 5 ms under 14 kV.

Combined with the mechanism of back discharge inside the accumulated bubble, there are two possible mechanisms for back discharge at the interface with the unrestricted bubbles, which is indicated in Fig. 16.

The streamer of a forward discharge, which propagates along

the ceramic surface inside the bubble, may leave ions on two interfaces: the vapor-ceramic interface and the vapor-liquid interface. First, different from the accumulated bubble, the vapor-ceramic interface will shifts to a liquid-ceramic interface once the bubble detaches from the surface. As shown in Fig. 16(a), The liquid environment would restrain the back discharge, even if the inversed field dominates and reaches the critical value. The back discharge may only occur once another bubble generates from the charged area. Therefore, the charged interface cannot modulate the electric field in successive periods. It can be analogized to the impact of the back discharge on the forward discharge.

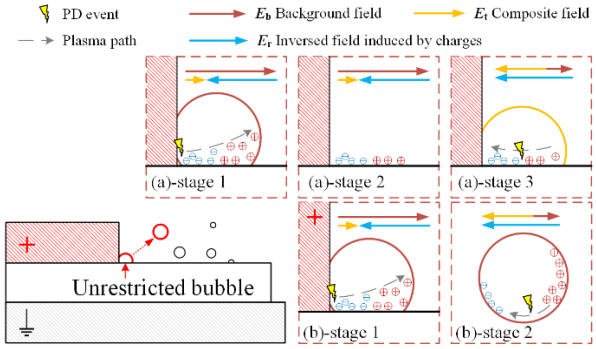

Fig. 16. Schematic diagram of back discharge in unrestricted bubbles at the interface.

Second, as indicated in Fig. 16(b), the ions may also attach to the vapor-liquid interface. The electric field in the bubble not only decreases with the period but also drops as the bubble leaves the ionization area. It is more likely to trigger a back discharge inside the bubble before reaching the liquid level. This can be confirmed by the crack of the bubble observed in Fig. 8. While, this charged interface cannot affect the electric field along the ceramic surface anymore.

Based on the mechanism analysis above, the charged interface cannot affect the forward discharge and the back discharge in successive voltage periods. The dynamic behaviors of the charged interface in two mechanisms can be proven by the statistics of t_r as Fig. 17.

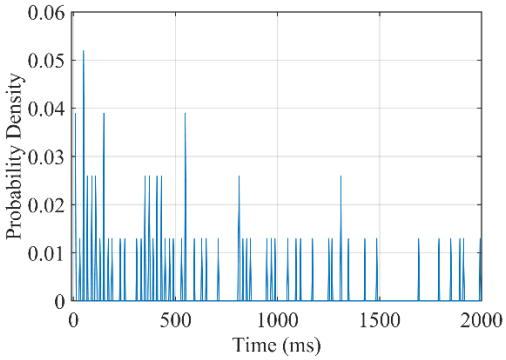

Fig. 17. Probability distribution of the t_r within the unrestricted bubbles.

In Fig. 17, only a few of back discharge can respond within 20 ms. The distribution of t_r is more scattered comparing with that in the accumulated bubble. The response time t_r here is determined by the time lag before the ionization inside the floating bubble, or the time interval between the bubbles appearing in one area. Since the bubble exists in liquid as longest as about 500 ms, the back discharge, whose response time is longer than 500ms, can only occur at the ceramic surface as the mechanism in Fig. 16(a).

V. Conclusions

In this paper, we focus on the characteristics of surface insulation in the two-phase immersion cooling. According to the contrastive analysis of PD in air, FC-72 liquid, and its boiling state, it reflects the insulation enhancement of the FC-72 environment and a certain degradation induced by bubble, which may be referable for the insulating evaluation of two-phase immersion cooling.

In order to reveal the discharge mechanism with different bubble behaviors, two methods for bubble generation proceed. It realizes a bubble-existing interface in two conditions, which are unrestricted bubble and the accumulated bubble. The differences of their PD features are analyzed and identified in their PRPD, PRPDN, and distribution of t_r.

Based on the bubble behaviors at the interface and the difference in PD patterns, the mechanism of back discharge inside the bubble is determined. For the interface with the accumulated bubble, the back discharge is still triggered as a classical surface discharge since the surface is quasi-covered by the vapor layer. However, the charged interface in unrestricted bubble is more dynamic. The liquid will restrain the back discharge if the bubble detaches from the surface, which makes it can only be triggered until another bubble grows from the charged surface. Moreover, it is speculated that the back discharge can also occur along the bubble surface when it leaves the ionization area, which can be testified by the distortion and split of the floating bubble.

References

[1] C. Qian, A. M. Gheitaghy, J. Fan, H, Tang, B, Sun, H, Ye and G, Zhang, 'Thermal Management on IGBT Power Electronic Devices and Modules', *IEEE Access*, vol. 6, pp. 12868-12884, Jan. 2018.

[2] P. Fu, Z. Zhao, X. Li, X. Cui, T. Wen, Z. Yang, S. Mo, P. Zhang, 'Partial discharge measurement and analysis in PPIs', *IET Power Electron.*, vol. 12, no. 1, pp.138-146, Dec. 2019.

[3] P. Fu, Z. Zhao, X. Cui, T. Wen, H. Wang, X. Li, P. Zhang, "Parital discharge measurement and analysis in high voltage IGBT module under DC voltage", *CESS J. Power Energy Syst.*, vol. 4, no. 4, pp. 513-523, Dec. 2018.

[4] J. H. Fabian, S. Hartmann, A. Hamidi, 'Partial Discharge Failure Analysis of AIN Substrates for IGBT Modules', *Microelectron. Reliab.,* vol. 44, no. 9, pp: 1425-1430, June 2004.

[5] S. M. Korobeynikov, A. V. Ridel, , D. A. Medvedev, D. I. Karpov, A. G. Ovesyannikov and M. B. Meredova, 'Registration and simulation of partial discharges in free bubbles at AC voltage',. *IEEE Trans. Dielectr. Electr. Insul.*, vol. 26, no. 4, pp. 1035-1042, Aug. 2019.

[6] M. Sato, A. Kumada., K. Hidaka., K. Yamashiro, Y, Hayase and T, Takano, 'Dynamic potential distributions of surface discharge in silicone gel', *IEEE Trans. Dielectr. Electr. Insul.*, vol. 22, no. 3, pp. 1733-1738, June 2015.

[7] H. Aamdan., M. S. Cha, 'Ignition modes of nanosecond discharge with bubbles in distilled water', *J. Phys. D-Appl. Phys.*, vol. 48, no. 40, p.405206, Sep. 2015.

[8] K. Tachibana, Y. Takekata, Y. Mizumoto, H. Motomura, M. Jinno, 'Analysis of a pulsed discharge within single bubbles in water under synchronized conditions', *Plasma Sources Sci. Technol.*, vol. 20, no. 3, p. 34005, Apr. 2011.

[9] W. Tian, K. Tachibana, M.J. Kushner, 'Plasmas sustained in bubbles in water: optical emission and excitation mechanisms', *J. Phys. D-Appl. Phys.*, vol. 47, no. 5, p. 55202, Dec. 2013.

[10] S. Mo, Z. Zhao, X. Li, X. Cui, J. Xu, J, Zhang, 'Partial discharge characteristics of bubble flow under AC non-uniform electric field in FC-72'. *IEEE Trans. Dielectr. Electr. Insul.*, vol. 27, no. 4, pp. 1119-1127, Aug. 2020,
[11] Z. Yang, X. Li, X. Meng, Z. Zhao, P. Fu, B. Zhai, X. Cui, 'The influence of frequency on the surface discharge characteristics of PEEK under positive repetitive square voltage', *High Volt.*, vol. 5, no. 6, pp. 669-678, June 2020.
[12] S. Nakamura., A. Kumada., K. Hidaka, M. Sato, Y. Hayase, S. Tkano, K. Yamashiro and T. Takano, 'Electrical treeing in silicone gel under repetitive voltage impulses', *IEEE Trans. Dielectr. Electr. Insul.*, vol. 26, no. 6, pp. 1919-1925, Dec. 2019.
[13] T. Lebey, D. Malec, S. Dinculescu, F. Breit and E. Dutarde, 'Partial discharges phenomenon in high voltage power modules', *IEEE Trans. Dielectr. Electr. Insul.*, vol. 13, no. 4, pp.810-819, Aug. 2006.
[14] H.A. Illias, G. Chen, P.L. Lewin, 'The influence of spherical cavity surface charge distribution on the sequence of partial discharge events', *J. Phys. D-Appl. Phys*., vol. 44, no. 24, p.245202, June 2011.
[15] M. Hara, M. Kubuki, 'Effect of thermally induced bubbles on the breakdown characteristics of liquid nitrogen', *IEE Proceedings A – Phys. Sci.*, vol. 137, no. 4, pp.209-216, July 1990.
[16] P. Wang, D. J. Swaffield, and P. L. Lewin, 'Thermal bubble motion in liquid nitrogen under non-uniform electric field', *IEEE Trans. Dielectr. Electr. Insul.*, vol. 15, no. (3), pp. 626-634, June 2008.
[17] H. A. Pohl, 'Some effects of nonuniform field on dielectrics', J. Appl. Phys., vol. 29, no. 8, pp. 1182-1188, Aug. 1958.

Shenyang Mo was born in Henan, China, in 1992. He received the B.Sc. degree in Electrical Engineering from North China Electric Power University, Beijing, China, in 2015. He is a Ph.D. candidate in North China Electric Power University now. His research interests includes electrical Insulation for high voltage device package, dielectric properties and partial discharge diagnostic in liquids.

Xuebao Li was born in Tianjin, China, in 1988. He received his B.Sc. degree and Ph.D degree in Electrical Engineering from North China Electric Power University, Beijing, China, in 2011 and in 2016, respectively. He is currently an associate professor at the School of Electrical and Electronic Engineering, North China Electric Power University. His research interests include the electromagnetic environment and electromagnetic compatibility in power systems, and insulation problems in high-voltage apparatus.

Zhibin Zhao was born in Hebei, China, in 1977. He received his Ph.D. degree in Electrical Engineering from North China Electric Power University, Baoding, China, in 2005. Currently, he is a Professor at the State Key Laboratory of Alternate Electrical Power System with Renewable Energy Sources, North China Electric Power University. His main research interests include computational electromagnetics and electromagnetic compatibility in power electronic

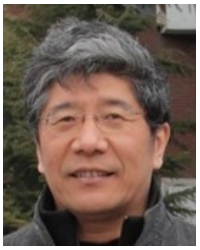

Xiang Cui (M'97–SM'98) was born in Baoding, Hebei Province, China, in 1960. He received his B.Sc. and M.Sc. degrees in Electrical Engineering from North China Electric Power University, Baoding, in 1982 and 1984, respectively, and his Ph.D. degree in Accelerator Physics from the China Institute of Atomic Energy, Beijing, China, in 1988. He is currently a Professor and the Vice Director of the State Key Laboratory of Alternate Electrical Power System with Renewable Energy Sources, North China Electric Power University. His research interests include computational electromagnetics, electromagnetic environment and electromagnetic compatibility in power systems, insulation and magnetic problems in high-voltage apparatus. Prof. Cui is a Standing Council Member of the China Electrotechnical Society, a Fellow of *IET*, a Senior Member of *IEEE*. He is also an Associate Editor of *IEEE Transactions on Electromagnetic Compatibility*